Journal of Zhejiang University-SCIENCE A (Applied Physics & Engineering)
ISSN 1673-565X (Print); ISSN 1862-1775 (Online)
www.zju.edu.cn/jzus; www.springerlink.com
E-mail: jzus@zju.edu.cn

A study of multi-pass scheduling methods for die-less spinning*

Hai GUO, Jin WANG†‡, Guo-dong LU, Zi-han SANG, Qi-hang WANG

(*State Key Laboratory of Fluid Power and Mechatronic Systems, Zhejiang University, Hangzhou 310027, China*)

†E-mail: dwjcom@zju.edu.cn

Received May 30, 2016; Revision accepted Aug. 13, 2016; Crosschecked May 9, 2017

Abstract: The multi-pass scheduling method is a key issue in die-less spinning for determining the quality of the final products, including their shape deviations and wall thicknesses, and has drawn increasing interest in recent studies devoted to trying to improve the accuracy of the formed parts. In this paper, two main parameters, roller path profiles and deformation allocations in each pass, are considered in newly proposed multi-pass scheduling and optimizing methods in die-less spinning. Four processing methods with different roller path profiles and with three deformation allocation methods are proposed for investigating the influence of scheduling parameters on product qualities. The 'similar geometry principle for restraining shape deviation' and the 'small curvature principle for maintaining wall thickness' are presented for optimal design of roller path profiles; in addition, the 'uniform allocation principle for maintaining wall thickness' and the 'large deformation principle for restraining shape deviation' are brought forward as suggestions for deformation allocations. Based on these principles, a scheduling method denoted by RF+(FP & EHS) is presented to improve the comprehensive quality of a product of die-less spinning.

Key words: Die-less spinning; Pass schedules; Shape deviations; Roller path profiles; Deformation allocations
http://dx.doi.org/10.1631/jzus.A1600403 **CLC number:** TG306

1 Introduction

Metal sheet spinning, due to its chip-less machining and material quality improving properties, plays an important role in the manufacture of aviation, space, and civilian products. However, the conventional spinning process is not strictly flexible because of its requirement for specific mandrels (Music *et al*., 2010), leading to long manufacture time and poor versatility of the process. Die-less spinning, on the other hand, is capable of increasing the flexibility of conventional spinning by removing the necessity for specific mandrels (Xia *et al*., 2014); it is thus widely regarded as a novel technology with high value both in research and in industrial applications.

The die-less spinning method has been in use for a long time and been much investigated. Many different products, such as fully symmetric conical ones (Kawai *et al*., 2001), truncated hemispherical shells (Kawai *et al*., 2007), and even asymmetric products with square sections (Jia *et al*., 2015), have been successfully formed by die-less spinning. Moreover, finite element numerical models have been satisfactorily built for this forming process (Liu, 2007).

In traditional spinning, the contour of the formed part is supported during forming by a mandrel with the same shape (Wong *et al*., 2003), and thus shape deviations in the formed parts are small enough to be neglected in most conditions. By contrast, in die-less spinning, the formed part cannot be supported by the general mandrel, resulting in more significant shape deviations which cannot be neglected. Hence, deep investigations of these shape deviations are necessary.

‡ Corresponding author

* Project supported by the Zhejiang Provincial Natural Science Foundation of China (No. LY15E050003), the National Natural Science Foundation of China (No. 51675470), and the Fundamental Research Funds for the Central Universities, China (No. 2015QNA4003)

ORCID: Hai GUO, http://orcid.org/0000-0003-1867-521X; Jin WANG, http://orcid.org/0000-0003-3106-021X

El-Khabeery *et al*. (1991) reported that the distribution of shape deviations is not uniform and is influenced by a series of process parameters, such as the roller face angle, feed rate, and roller nose radius. Kang *et al*. (1999) pointed out that the border of a spun part has the higher shape deviation because of the relatively low stability in that area. Quigley and Monaghan (2000) investigated the effects of the pass number on shape deviations, with the results indicating that the shape deviations of the formed parts formed by single-pass schedules are larger than those formed by multi-pass ones. Li *et al*. (2014) indicated that shape deviations of the formed parts using die-less spinning are related to the geometries of the roller path profiles, a result supported by the conclusions in Polyblank and Allwood (2015).

These results suggest that the influence of multi-pass schedules on shape deviations of formed parts is important in die-less spinning. However, systematic research on multi-pass scheduling methods in die-less spinning is still inadequate. Existing related publications on pass schedules focused mainly on traditional spinning.

Hayama *et al*. (1970) proposed a pass scheduling method according to the revolving angles and pass pitches of the roller path profiles. In their study, pass schedules were classified into two types, revolved and shifted ones, both of which have been proved to be capable of forming suitable products. Their result was referenced by Sugita and Arai (2015) for pass scheduling in synchronous spinning, with their results indicating that wall thickness distributions are similar when using rotational and translational pass sets, e.g., revolved and shifted type pass schedules in Hayama *et al*. (1970), in the forming of circular cup shapes.

Lin *et al*. (2015) compared different patterns of deformation allocations and concluded that deformation allocation has significant effects on the quality of formed parts in multi-pass spinning, including wall thickness, fittability, and strain distribution. Wang and Long (2013) reported that a multi-pass schedule without tool compensation leads to wrinkling failures, which do not occur if tool compensation is taken into account.

It can be found in the above publications that roller path profiles were designed theoretically and independently, without consideration of their relationship with the desired shape of products. Furthermore, involute path profiles were suggested to be applied in the passes before the desired contour was formed, e.g., the former passes in this study, because of their advantages in reducing spinning force and maintaining wall thickness (Hayama *et al*., 1970; Liu *et al*., 2002; Music *et al*., 2010; Wang and Long, 2011).

On the other hand, the effects of roller paths on shape deviations of the formed parts in die-less spinning have not been fully analyzed and verified. Consequently, more work needs to be done in roller path design, as it may be closely related to the desired shapes of products in die-less spinning.

Therefore, we propose a new multi-pass scheduling method for die-less spinning based upon detailed studies of roller path profiles and deformation allocations, in order to help achieve good product qualities for die-less spinning and to assist in its further industrial application.

2 Investigations of roller path profiles

2.1 Classification of roller path profiles

As mentioned before, there are mainly two types of processing methods, i.e., revolved and shifted ones (Fig. 1). In shifted spinning, the blank will be attached to the mandrel in the process of every pass, making the whole forming process more dependent on the mandrel. By contrast, in revolved type spinning, it is only in the final pass that the blank is attached to the mandrel.

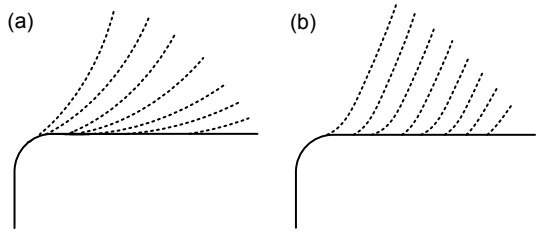

Fig. 1 Revolved (a) and shifted (b) types of roller path profiles of traditional spinning (Hayama *et al.*, 1970)

As a result, four processing methods, i.e., FF-inv (the final-pass forming method with involute roller paths used in former passes), FF-lin (the final-pass forming method with straight line roller paths

used in former passes), GF (the gradual forming method), and RF (the revolved forming method), will be developed from the revolved type, which is more suitable for die-less spinning; detailed settings of the four derived processing methods are described in Table 1.

2.2 Experimental studies on roller path profiles

2.2.1 Experiment settings

1. Material and parameters

The blank sheets used in the experiments were cut from commercial SPHC steel plates, with the diameter of 240 mm and thickness of 1.9 mm; the diameter of the general mandrel was 80 mm; the dimension of the roller is shown in Fig. 2; the feed ratio was 0.25 mm/r and the rotational speed of the mandrel was 400 r/min.

2. Coordinate systems

The global coordinate system *O*-*yz* is illustrated in Fig. 2, in which the *z*-axis overlaps the rotation axis of the general mandrel with its positive direction pointing to the general mandrel; the *y*-axis and *z*-axis are in the shared symmetrical plane of the general mandrel, the blank, and the roller; and the positive direction of the *y*-axis is pointed to the outline of the general mandrel. In addition, the roller path coordinate

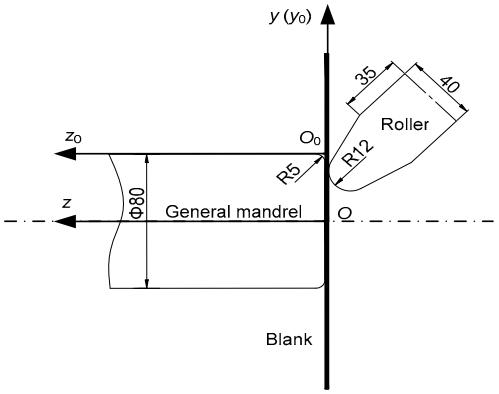

Fig. 2 Schematic diagram of die-less spinning experiments (unit: mm)

Table 1 Processing methods with different roller path profiles

Processing method	Former-pass roller path[a]	Final-pass roller path	Schematic[b]	Note
FF-inv: final-pass forming (involute in former passes)	Involute	Desired shape	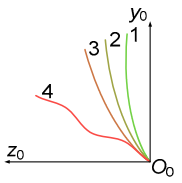	Involute roller paths, which have proved best in traditional spinning, are applied as roller paths in former passes
FF-lin: final-pass forming (line in former passes)	Straight line	Desired shape	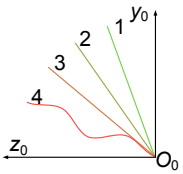	Roller paths in former passes are straight lines
GF: gradual forming	Gradually transits from a straight line to the desired shape	Desired shape	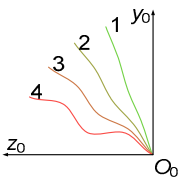	Former-pass roller paths are between straight lines and the desired shape
RF: revolved forming	Desired shape	Desired shape	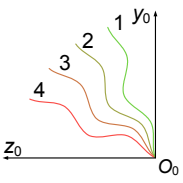	Roller path profiles are identical to the desired shape

[a] Former passes refer to the passes before the final one; [b] The roller path coordinate system O_0-y_0z_0 is shown in Fig. 2 (the numbers represent the pass sequence: '1' is the first pass and '4' is the final pass)

system O_0-y_0z_0 is built with the position and direction of the y_0-axis identical to the y-axis; the z_0-axis is placed on the contour line of the general mandrel and its direction is identical to the z-axis.

3. Roller paths

In this study, the slant angle refers to the angle between the centerline of the roller path profile and the y-axis, as demonstrated in Fig. 3.

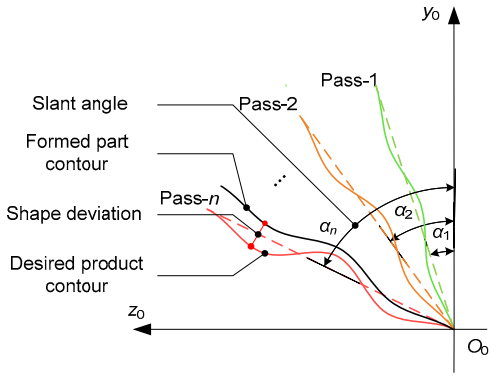

Fig. 3 Schematic diagram of roller paths, slant angles, and shape deviations

The experiments on forming products with complex contours, in which different processing methods were used, were carried out with four forward passes; the slant angles were 20°, 30°, 40°, and 50°; the geometry of the contour of the desired part was irregular and is displayed in Fig. 4. It is identical to the profile of the final-pass roller path.

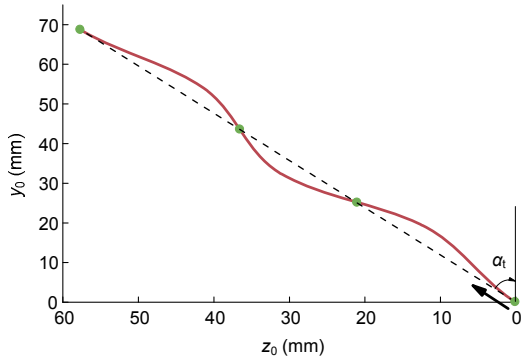

Fig. 4 Profile of the final-pass roller path, identical to the desired part contour (α_t is the slant angle of the desired part contour)

The slant angles of the former passes were designed by reference to the traditional pass scheduling method (denoted by the TRA method in this study) proposed by Hayama *et al.* (1970), according to which the first-pass angle is larger than the other passes while the angle differences are uniform between the passes. Moreover, as increased numbers of passes would reduce the productivity of the spinning processes, scheduling methods are discussed under the condition of constant four passes.

4. Feed directions

In this study, backward passes are not taken into consideration for the purpose of focusing on the influences of roller path profiles and deformation allocations. Additionally, thinning of the part wall would be more serious if only forward passes were applied, and this is a benefit for distinguishing the effects of scheduling methods on maintaining the thickness of the part wall.

5. Quality evaluation indicators

For the purpose of comparing the effects of different schedules, as shown in Fig. 3, the distance between the spun product contour and the desired part contour is defined as the shape deviation, taken as a quantitative evaluation criterion of the quality of the product, along with its part wall thickness.

6. Measurement of indicators

To obtain the shape deviations of spun products, the geometries of the spun parts were first measured by the device displayed in Fig. 5a; then shape deviations were acquired by comparing the contour of the spun part with that of the desired product.

As illustrated in Fig. 5b, a displacement sensor was fixed on an electric slider which was driven by a linear motor. During the measurement process, the displacement sensor was moved with the slider in a constant speed, of which the moving distance along the y-direction was ΔL in one sampling period. Meanwhile, the probe of the sensor was moved on the part surface towards the brim along a radius of the spun part, collecting Δz_s, which is the extending distance of the probe of sensor, at a fixed sample frequency, high enough to obtain the details of the product shape.

The coordinates of a sample point P_{j+1} could be obtained from a previous point P_j according to the geometric relationship. The contour of the spun part was obtained as follows:

$$\begin{cases} z_{j+1} = z_j + \Delta z = z_j + \Delta z_s \cos\theta, \\ y_{j+1} = y_j + \Delta y = y_j + \Delta L - \Delta z_s \sin\theta, \end{cases} \tag{1}$$

where θ is the inclination angle of the displacement sensor designed to prevent the probe from unacceptable deflection, y_j and z_j are the y and z coordinates of point P_j, respectively, $\Delta z=z_{j+1}-z_j$, and $\Delta y=y_{j+1}-y_j$.

For the wall thickness measurement, a PX-7 supersonic thickness gauge was applied (Fig. 6). When measuring the spun parts with complex contours, the probe was first moved back and forth along the radius (marked in red in Fig. 6), to search for the points with extreme values of wall thickness in the local area. After all the local thickness extreme points were found, other sample points on the same radius were then measured with the radial interval between two sample points generally larger than 10 mm. In that way, the general characteristics of wall thicknesses could be obtained and the extreme values of thickness would not be omitted. When the generatrix of the measured part was a straight line, the radial interval between two sample points would be a fixed value at 10 mm.

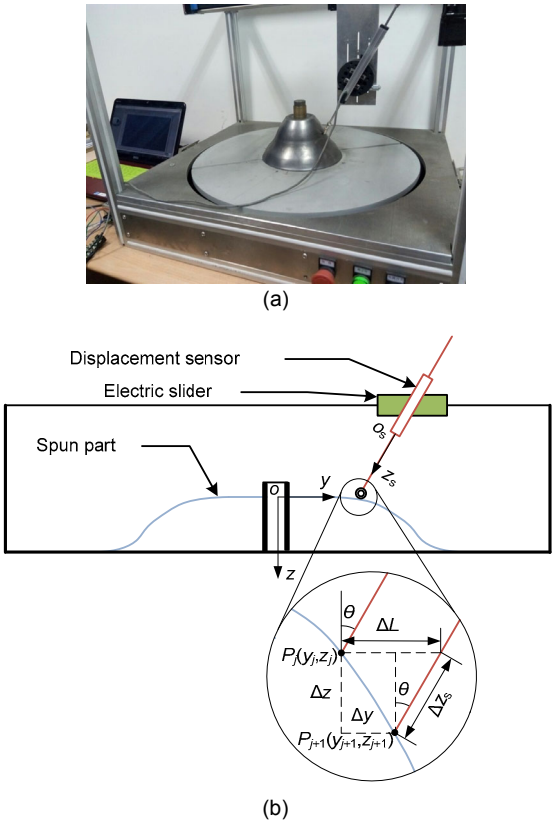

Fig. 5 Measurement of part contour
(a) Measuring device; (b) Measurement schematic of part contour

Fig. 6 Measurement of wall thickness of spun parts (references to color refer to the online version of this figure)

2.2.2 Results and discussion

1. Shape deviations

According to Fig. 7, in which the mean value μ is illustrated with colored bars and the standard deviations σ are illustrated with vertical lines, the shape deviation of the spun part using the RF method is smaller than those using other methods. As the elastic energy of the blank was released after the roller

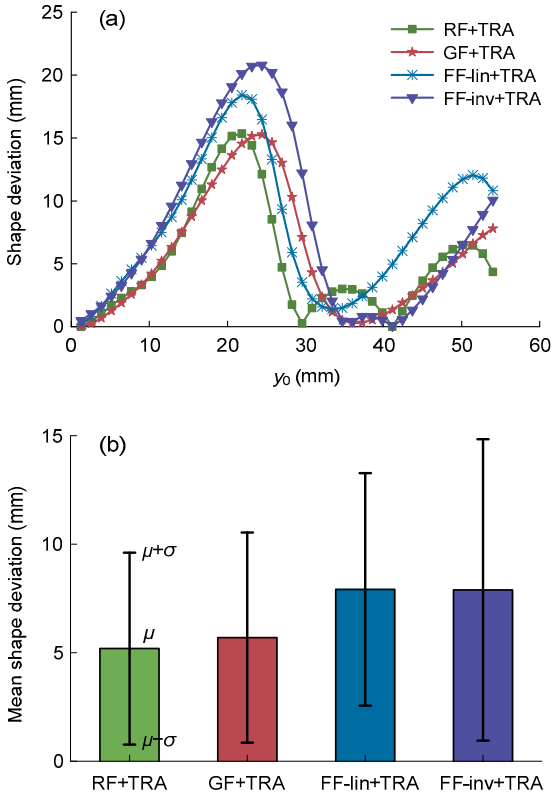

Fig. 7 Shape deviations of the parts under different processing methods
(a) Distribution of shape deviations in the radial direction; (b) Mean values and standard deviations of shape deviations

left the blank with the blank shape gradually 'approaching' the desired shape in each pass, the impact of springback deformation was lessened and so the shape deviation was reduced.

By contrast, as shown in Fig. 7, the shape deviation of the FF-inv method was the largest, which can be attributed to the large gap between the shape of its roller path and the desired shape. In other words, the blank was 'forced' to the desired shape in the final pass. Thereby springback deformation in the final pass was increased, and hence a larger shape deviation was produced.

As a conclusion, by using a roller path with similar geometry to the desired product contour, shape deviations of formed parts can be reduced; this is called the 'similar geometry principle for restraining shape deviation' in this study.

2. Part wall thicknesses

It is illustrated in Fig. 8 that the wall thickness of the spun part using the FF-inv method was better maintained.

Considering that the thinning of the part wall is accumulated in each pass of a spinning process, the roller path profile of each pass has an impact on the thickness of the part wall. Taking the RF method as an example, because the roller path profile had a larger curvature and more complex concave-convex curves, the metal flow was enhanced due to the complex geometry of the roll path and so the part wall thinning was aggravated.

In contrast, as shown in Fig. 8, the use of the involute roller path, as well as the linear one, both of which are composed of small curvature curves, will help prevent excessive thinning of the part wall.

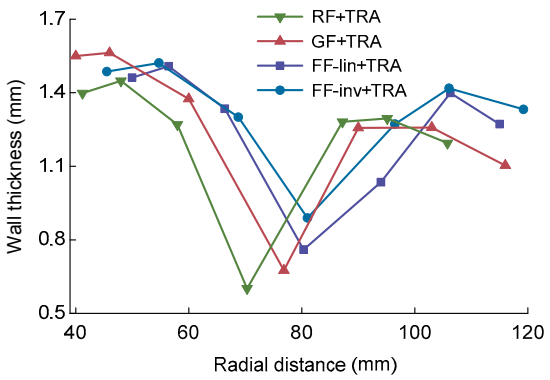

Fig. 8 Wall thicknesses of the parts under different processing methods

Thus, to keep the part wall from excessive thinning, it is necessary to use a small curvature in roller path design and this is called the 'small curvature principle for maintaining wall thickness'.

3. Failures

As shown in Fig. 9, the bottom region held by the blank holder was cut from the blank when the FF-inv method was used; and circumferential cracking occurred when the RF method was applied; by contrast, there was no failure when the FF-lin or GF method was used. The spun parts in Fig. 9 were produced with slant angle of 30°, 40°, 50°, or 60°; in addition, the desired contour geometry of the part is illustrated in Fig. 4 with α_t (the slant angle of the desired part contour) as 60°.

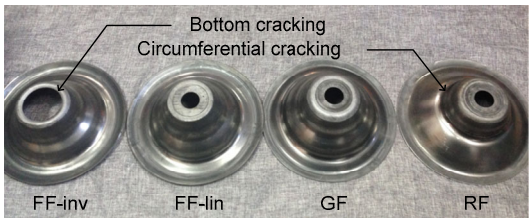

Fig. 9 Part qualities formed under different processing methods

According to Table 1, final-pass deformation in the FF-inv method is the largest in the four processing methods, especially on the flange side. Moreover, as a large deformation will lead to a large spinning force, bottom cracking failure happened when the FF-inv method was used. Besides, as the wall was excessively thinned during the spinning process, circumferential cracking occurred on the part wall when the RF method was used.

4. Conclusions

According to the above analyses, the roller path profile will influence both the shape deviation and the wall thickness and, for the purpose of reducing the shape deviation, the roller path should be designed with its profile similar to the desired product contour according to the 'similar geometry principle for restraining shape deviation'. To keep the part wall from excessive thinning, the curvature roller path profile should be small according to the 'small curvature principle for maintaining wall thickness'. The above conclusions are demonstrated in Table 2.

According to Table 2, the RF method has an advantage in respect of restraining shape deviation

but a disadvantage in maintaining wall thickness. Given that shape precision of spun parts is difficult to control in die-less spinning because the blank lacks the support of the traditional mandrel, the RF method was applied in the later research described in this study.

Table 2 Comparison of formed part qualities of different processing methods

Method	Shape precision	Wall thickness keeping capability
FF-inv	−−	++
FF-lin	−	+
GF	+	−
RF	++	−−

'+' is used if the method has a positive effect on the product quality and '−' if the effect is negative

3 Deformation allocation methods

3.1 Equal pass angle allocation method

In the existing publications, the deformation allocation is usually designed according to the slant angle of the roller path profile, which cannot precisely quantify the deformation of a spinning process, especially when the curvature of the roller path profile is variable.

For instance in Fig. 10, the amount of deformation of curve 2a is less than that of curve 2b although the slant angles of the two curves are identical ($\Delta\alpha$). This is caused by the different profiles of the two roller paths.

Thus, slant angles cannot accurately quantify deformations of roller paths with various curvatures; the equal pass angle (EPA) allocation method cannot allocate deformation evenly (Fig. 11).

3.2 Equal diameter decrement allocation method

Besides the slant angle, the blank diameter is another important factor for measuring deformation. The equal diameter decrement (EDD) allocation method based on the diameter decrement ΔD is illustrated in Fig. 12:

$$\Delta D=D_i-D_{i+1}, \tag{2}$$

where D_i refers to the blank diameter after pass-i.

The blank diameter decrement also cannot precisely quantify the deformation. As illustrated in Fig. 10, the deformation of curve 2a is less than that of curve 2c although the diameter decrements of these two curves are identical (ΔD). As a result, the EDD allocation method also cannot allocate the deformation evenly.

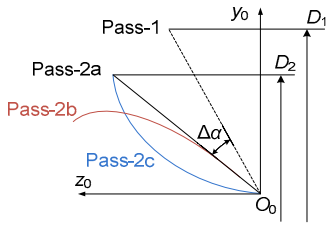

Fig. 10 Different roller path profiles with identical slant angles or diameters

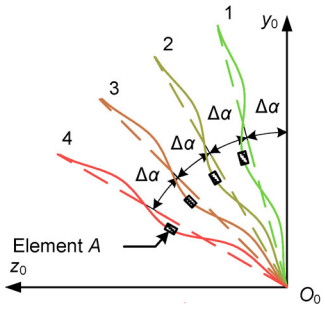

Fig. 11 Schematic diagram of the RF+EPA allocation method

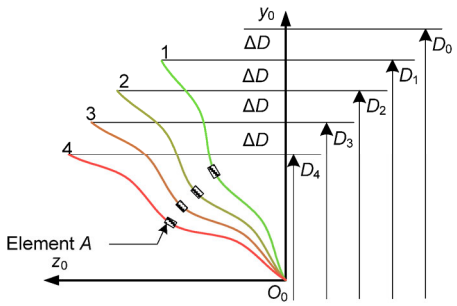

Fig. 12 Schematic diagram of the RF+EDD allocation method

3.3 Equal hoop strain allocation method

It is accepted that the main character of a conventional spinning process is to reduce the diameter of the blank (Music *et al.*, 2010). Likewise, the main purpose of deformation in multi-pass die-less

spinning is to alter the diameter of the blank; accordingly, a novel deformation allocation method based on the average hoop strain $\bar{\varepsilon}_{\mathrm{h}}$ is proposed in this study.

The mechanism of dimension change of a blank in die-less spinning was demonstrated in Fig. 13, in which the blank contours before and after spinning are displayed with blue and red colors, respectively. As shown in Fig. 13, the hoop strain of element i, i.e., the variation of its perimeter, can be calculated by

$$\varepsilon_{\mathrm{h}}=\int_{2\pi r_i}^{2\pi R_i}\frac{\mathrm{d}l}{l}=\ln\frac{2\pi R_i}{2\pi r_i}=\ln\frac{R_i}{r_i}, \tag{3}$$

where r_i and R_i are respectively the radial positions of the hoop element i before and after deformation. Therefore, the diameter reduction of element i can be quantified by its hoop strain.

Similarly, deformation can be quantified by the average hoop strain $\bar{\varepsilon}_{\mathrm{h}}$ of the blank given by

$$\bar{\varepsilon}_{\mathrm{h}}=\int_{\bar{r}}^{\bar{R}}\frac{\mathrm{d}r}{r}=\ln\frac{\bar{R}}{\bar{r}}=\ln\frac{2\bar{R}}{2\bar{r}}=\ln\frac{\bar{d}'_n}{\bar{d}_1}, \tag{4}$$

where $\bar{r}$ and $\bar{R}$ are respectively the average diameter dimensions of the blank before and after spinning, as demonstrated in Fig. 13. We have $\bar{d}_1=2\bar{r}$ and $\bar{d}'_n=2\bar{R}$, respectively the average diameters of the blank before pass-1 and after pass-n. Moreover, $\bar{r}$ can be calculated by the integration method:

$$\bar{r}=\frac{\int_0^{z_1}f(z)\mathrm{d}z}{z_1}, \tag{5}$$

in which $D=f(z)$ is the equation of the roller path profile.

The average hoop strain of the blank in pass-i can be calculated by

$$\bar{\varepsilon}_{\mathrm{h}i}=\ln\frac{\bar{d}'_n}{\bar{d}_i}. \tag{6}$$

Since $\bar{d}_i=\bar{d}'_{i-1}$, the relationship between the deformation of the whole spinning process and pass-i can be given by

$$\begin{aligned}\bar{\varepsilon}_{\mathrm{h}}&=\ln\frac{\bar{d}'_n}{\bar{d}_1}=\ln\left(\frac{\bar{d}_2}{\bar{d}_1}\frac{\bar{d}_3}{\bar{d}_2}\cdots\frac{\bar{d}'_n}{\bar{d}_n}\right)\\&=\ln\left(\frac{\bar{d}'_1}{\bar{d}_1}\frac{\bar{d}'_2}{\bar{d}_2}\cdots\frac{\bar{d}'_n}{\bar{d}_n}\right)=\sum_{i=1}^{n}\bar{\varepsilon}_{\mathrm{h}i}.\end{aligned} \tag{7}$$

Consequently, in the equal hoop strain (EHS) method, as the deformation quantity is related to the roller path profile, the accuracy is better than those in the EPA and EDD allocation methods, especially for spinning processes with complex roller path profiles. The EHS method based on average hoop strain is displayed in Fig. 14, and can be expressed by

$$\bar{\varepsilon}_{\mathrm{h}1}=\bar{\varepsilon}_{\mathrm{h}2}=\ldots=\bar{\varepsilon}_{\mathrm{h}n}=\frac{1}{n}\bar{\varepsilon}_{\mathrm{h}}. \tag{8}$$

In the form of average diameter, it can also be given by

$$\ln\frac{\bar{d}'_1}{\bar{d}_1}=\ln\frac{\bar{d}'_2}{\bar{d}_2}=\ldots=\ln\frac{\bar{d}'_n}{\bar{d}_n}=\frac{1}{n}\ln\frac{\bar{d}'_n}{\bar{d}_1}. \tag{9}$$

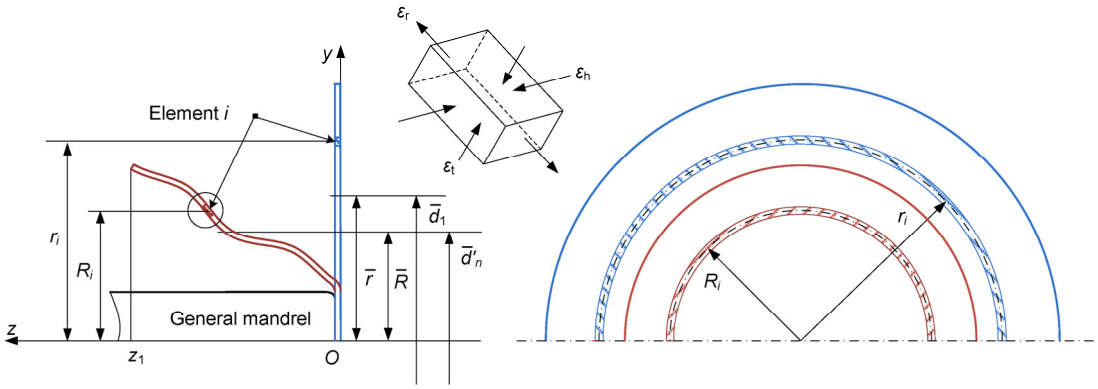

Fig. 13 Schematic diagram of blank deformation in die-less spinning (references to color refer to the online version of this figure)

To show the specific differences from the application of different deformation allocation methods, the proposed methods were applied to the schedule of the RF method and the slant angles obtained are shown in Table 3, in which α_i refers to the slant angle of pass-*i*.

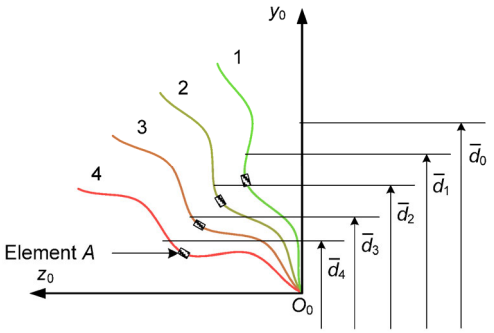

Fig. 14 Schematic diagram of the RF+EHS allocation method

Table 3 Slant angles of roller paths using different pass scheduling methods

Method	Slant angle (°)			
	α_1	α_2	α_3	α_4
RF+EPA	12.5	25.0	37.5	50.0
RF+EDD	23.0	35.0	43.0	50.0
RF+EHS	28.0	36.0	44.0	50.0

4 Effects of deformation allocations on shape deviations

4.1 Experimental results of shape deviations

The experiments, displayed in Fig. 4, on the forming of parts with complex contours, using the EPA, EDD, and EHS allocation methods, were carried out with four passes, for which α_t was 50°. The slant angles of the roller path profiles are illustrated in Table 3.

As demonstrated in Fig. 15, the order of shape deviations of spun parts is EHS>EDD>EPA. As its final-pass deformation is the largest among the three, the shape deviation of the spun part is best restrained when the EPA method was applied, given that the proportion of springback deformation was reduced and thus the impact of springback to the product contour was diminished.

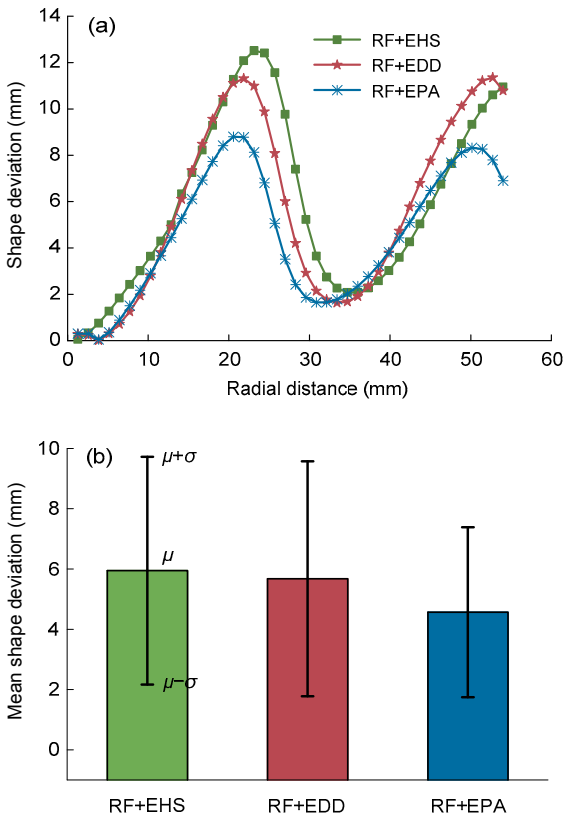

Fig. 15 Shape deviations using different deformation allocation methods

(a) Shape deviations along the radial direction; (b) Mean values and standard deviations of shape deviations

4.2 Theoretical analysis on effects of deformation allocations on shape deviations

First, the strain ε will be increased with the increment of deformation. The proportion of elastic strain η_E can be calculated by

$$\eta_E=\varepsilon_E/(\varepsilon_P+\varepsilon_E), \tag{10}$$

where ε_E is the elastic strain and ε_P is the plastic strain. Similarly, the proportion of plastic strain η_P can be calculated by

$$\eta_P=\varepsilon_P/(\varepsilon_P+\varepsilon_E). \tag{11}$$

The elastic strain increment $\Delta\varepsilon_E=\varepsilon_{E2}-\varepsilon_{E1}$ is negligible when it is compared with the plastic strain increment $\Delta\varepsilon_P=\varepsilon_{P2}-\varepsilon_{P1}$, especially for an ideal blank material with a large Young's modulus and a low hardening tendency. As shown in Fig. 16b, η_E is

decreased as ε_P gets larger. As springback deformation will alter the contour of a spun part, when the proportion of elastic deformation is decreased by η_E, the shape deviation brought about by springback deformation is reduced.

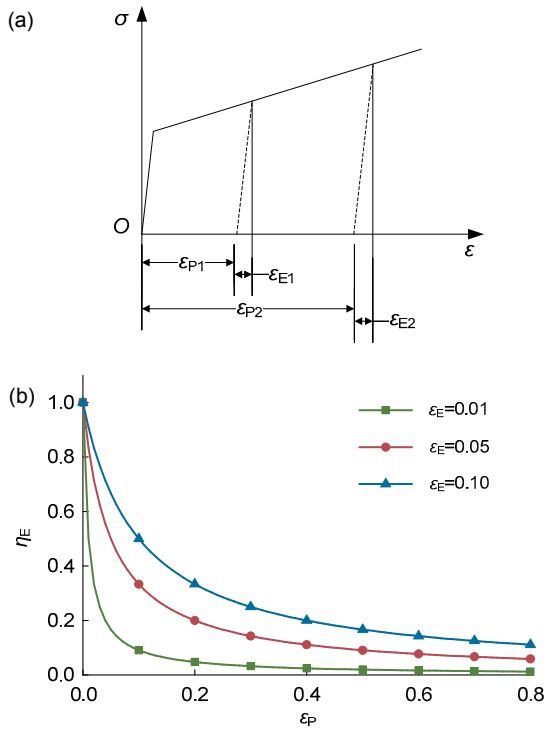

Fig. 16 Relationship between plastic strain and elastic strain proportions

(a) Deformation behavior of ideal linear hardening metals (Kopp and Wiegels, 1998); (b) Relationship between plastic strain and elastic strain proportions ignoring elastic strain increment

In conclusion, when deformation is increased, the shape deviation will be decreased as springback is restrained.

For the purpose of confirming the validity of the above theoretical analysis, forming experiments were conducted with single-pass schedules, of which the roller path profiles are demonstrated in Fig. 4.

According to Fig. 17, when the slant angle of the roller path profile α_t was increased from 20° to 40°, the difference between α_t and the slant angle of the spun part contour α'_t was reduced from 2.9° to 1.3°; additionally, the shape deviation was reduced. As ε_E and deformation were increased with α_t, the springback deformation was reduced, resulting in a reduction of shape deviation. So far, the validity of theoretical analysis has been verified.

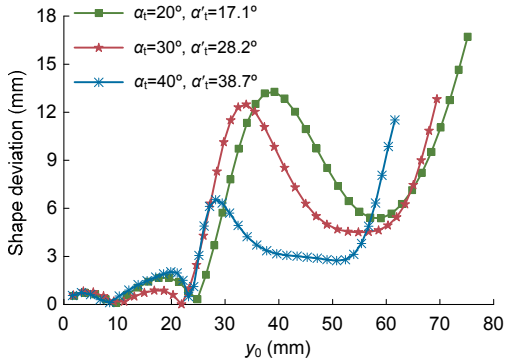

Fig. 17 Shape deviations of formed parts under different roller path slant angles

As the final-pass deformation was the largest when the EPA allocation method was applied, its shape deviation was best restrained, as shown in Fig. 15. In that case, for the purpose of reducing the shape deviation, a reasonably large deformation is essential and this is called the 'large deformation principle for restraining shape deviation' in this study.

5 Effects of deformation allocation methods on part wall thickness

5.1 Experimental results of part wall thickness

As illustrated in Fig. 18, the part wall thickness was better maintained when the EHS method was used; by contrast, the part wall was severely thinned when the EPA method was applied.

This is because the part wall thickness can be better maintained when deformation is evenly spread among the passes, and, by contrast, the part wall will be seriously thinned if deformation does not occur uniformly across the passes.

5.2 Theoretical analysis on effects of deformation allocations on wall thickness

Deformation of blank material may be separated into hoop, radial, and thickness strains. Besides the hoop strain which was analyzed in Section 3.3, the thickness strain, as its name suggests, represents the

variation of normal distance between the upper and lower surfaces of the wall as demonstrated in Fig. 13. Similarly, the radial strain is in the direction which is tangential to the contour of the part and lies in the axial-section plane.

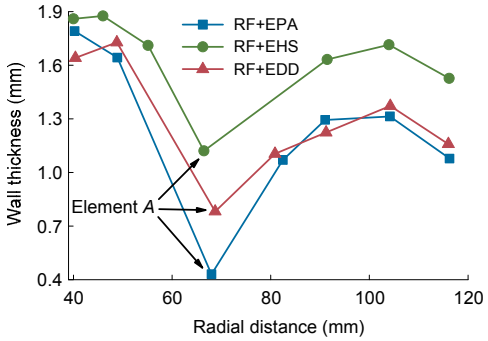

Fig. 18 Wall thicknesses of the parts using different deformation allocation methods

In a die-less spinning, the hoop strain is determined by the geometry of the roller path. Thickness and radial strains can be considered as the result of the designed hoop strain and the forming properties of the material.

For the purpose of proving the inference of Section 5.1 theoretically, a spinning process with two passes was taken as an example for analysis. When the hoop strains of the two passes are identical, i.e.,

$$\varepsilon_{h1}=\varepsilon_{h2}=\varepsilon_{h0}, \tag{12}$$

where ε_{hi} is the hoop strain of pass-*i*.

According to volume constancy, relationships among the three strains can be expressed by (Kopp and Wiegels, 1998)

$$\varepsilon_t+\varepsilon_h+\varepsilon_r=0. \tag{13}$$

Therefore, the thickness strains of two passes can be calculated by

$$\varepsilon_{t1}=-(\varepsilon_{h0}+\varepsilon_{r1}), \tag{14}$$

$$\varepsilon_{t2}=-(\varepsilon_{h0}+\varepsilon_{r2}), \tag{15}$$

$$\varepsilon_t=(\varepsilon_{t1}+\varepsilon_{t2})=-(2\varepsilon_{h0}+\varepsilon_{r1}+\varepsilon_{r2}). \tag{16}$$

By contrast, when hoop strains are not identical between the two passes, and assuming the difference between the hoop strains of the two passes is $2\Delta\varepsilon_h$, we have

$$\varepsilon'_{h1}-\varepsilon'_{h2}=2\Delta\varepsilon_h. \tag{17}$$

Since the total hoop strain is constant, there is

$$\varepsilon'_{h1}+\varepsilon'_{h2}=\varepsilon_{h1}+\varepsilon_{h2}=2\varepsilon_{h0}. \tag{18}$$

According to Eqs. (17) and (18), the hoop strains of two passes can be given by

$$\varepsilon'_{h1}=\varepsilon_{h0}+\Delta\varepsilon_h, \tag{19}$$

$$\varepsilon'_{h2}=\varepsilon_{h0}-\Delta\varepsilon_h. \tag{20}$$

Thus, the thickness strains of these two passes with different hoop strains can be written as

$$\varepsilon'_{t1}=-(\varepsilon'_{h1}+\varepsilon'_{r1})=-(\varepsilon_{h0}+\Delta\varepsilon_h+\varepsilon'_{r1}), \tag{21}$$

$$\varepsilon'_{t2}=-(\varepsilon'_{h2}+\varepsilon'_{r2})=-(\varepsilon_{h0}-\Delta\varepsilon_h+\varepsilon'_{r2}), \tag{22}$$

$$\varepsilon'_t=\varepsilon'_{t1}+\varepsilon'_{t2}=-(2\varepsilon_{h0}+\varepsilon'_{r1}+\varepsilon'_{r2}). \tag{23}$$

The difference of total thickness strains between the whole processes under different and identical hoop strains can be evaluated by

$$\Delta\varepsilon_t=\varepsilon'_t-\varepsilon_t. \tag{24}$$

Substituting Eqs. (16) and (23) into Eq. (24) yields

$$\Delta\varepsilon_t=(\varepsilon_{r1}+\varepsilon_{r2})-(\varepsilon'_{r1}+\varepsilon'_{r2}). \tag{25}$$

It should be noticed that, since the blank is compressed in the hoop direction and stretched in the radial direction (Quigley and Monaghan, 2000), all the hoop strains in Eqs. (12)–(25) are supposed to be negative and the radial strains are positive, except for the incremental quantities with the 'Δ' symbol.

The deformation process of the element is illustrated in Fig. 19. When $\Delta\varepsilon_h>0$, as $\varepsilon_{h0}<0$, $\varepsilon'_{h2}<\varepsilon_{h0}<\varepsilon'_{h1}<0$ could be obtained according to Eqs. (19) and (20). As $\varepsilon_{h0}<\varepsilon'_{h1}<0$, the size variation of the element in the hoop direction is decreased in pass-1 (Figs. 19a and 19c), which suggests that deformation is lessened in pass-1. Similarly, we can

obtain $\varepsilon'_{h2} < \varepsilon_{h0} < 0$, which implies that deformation is enhanced in pass-2.

We suggest that the dimensional change of an element could be separated into two steps, as displayed in Fig. 19a. In the first step, the element is compressed in the hoop direction under the hoop-direction roller force F_{h1}; meanwhile, material flows in the radial direction, causing strains ε_{h0} and ε_{r1_0}. In the second step, since material flows in the radial direction, the element will be stretched in the radial direction for a further radial strain ε_{r1} under the radial-direction force F_{r1}; meanwhile, the element will be compressed in the thickness direction.

Since the deformation is lessened in pass-1 and enhanced in pass-2 under different hoop strains (Figs. 19c and 19d), the increased deviation of deformation amount between the passes would enlarge deformation resistance for pass-2, and hence, disparities of roller forces between the passes would be widened, i.e., $F'_2 - F'_1 > F_2 - F_1$, or $\Delta F' > \Delta F$ in incremental form. Specific explanation on this part is given later and illustrated through finite element analysis (FEA).

Furthermore, the widening of the disparity of the roller forces between the passes would intensify radial-direction material flow and cause an extra addition of total radial strain. Hence, the following inequality could be obtained:

$$\varepsilon'_{r1} + \varepsilon'_{r2} > \varepsilon_{r1} + \varepsilon_{r2} > 0. \tag{26}$$

Substituting inequality (26) into Eq. (25), we have

$$\Delta\varepsilon_t<0. \tag{27}$$

Similarly, when $\Delta\varepsilon_h<0$, $\varepsilon'_{h1} < \varepsilon_{h0} < \varepsilon'_{h2} < 0$ can be obtained. It suggests that deformation is increased in pass-1 and decreased in pass-2, from which we can infer that $\varepsilon'_{r1} + \varepsilon'_{r2} > \varepsilon_{r1} + \varepsilon_{r2} > 0$. On the basis of our assumption, substituting the above into Eq. (25), $\Delta\varepsilon_t<0$ is still valid.

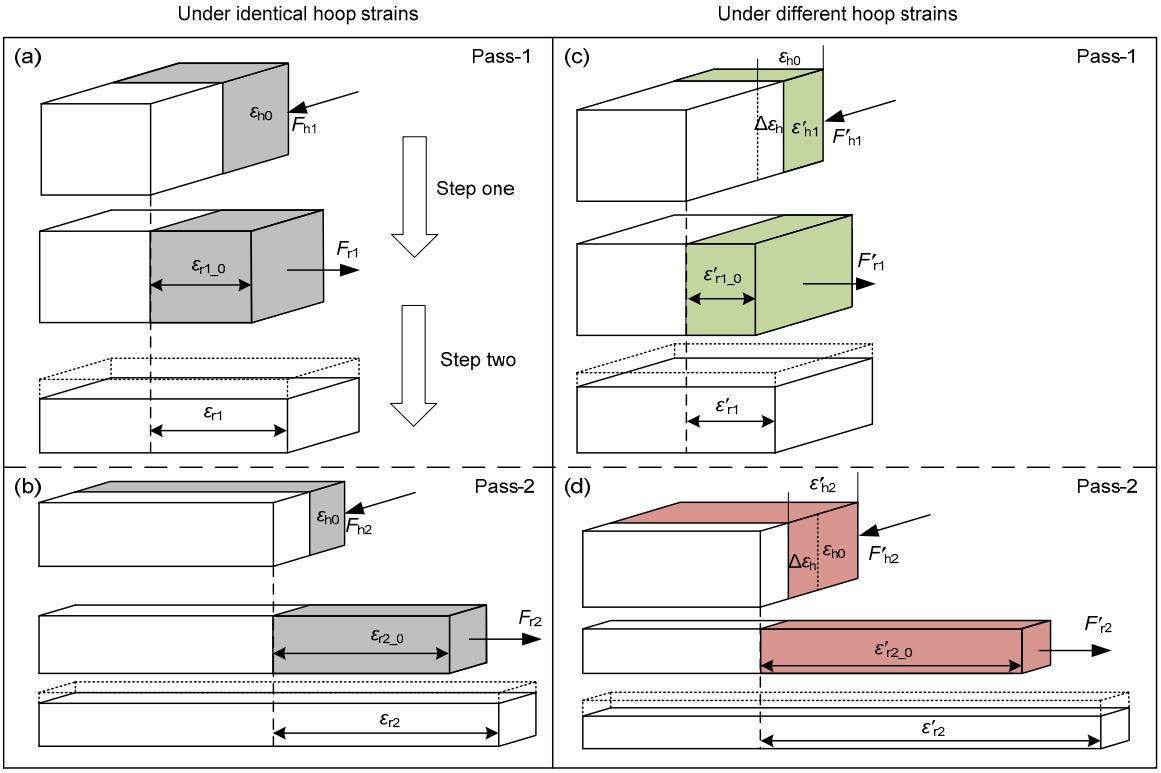

Fig. 19 Schematic diagram of dimensional change and deformation processes of an element under identical and different hoop strains in two passes

(a) First pass under identical hoop strains; (b) Second pass under identical hoop strains; (c) First pass under different hoop strains; (d) Second pass under different hoop strains

In summary, since the part wall is commonly thinned in die-less spinning, the following inequality can be inferred according to Eq. (24):

$$\varepsilon_t' < \varepsilon_t < 0, \tag{28}$$

which means that thinning of the part wall will be enhanced when hoop strains are not identical between the passes.

To verify the above speculations about roller forces and strains, FEA models were built based on commercial software LS-DYNA, of which the roller forces were demonstrated in Fig. 20. Stages I and II were the time periods when element A was deformed in pass-1 and pass-2, $\overline{F}_{\mathrm{I,EHS}}$ was the average roller force in Stage I when the EHS method was applied; $\varepsilon_{\mathrm{h1,EHS}}$ was the hoop strain of element A in pass-1 when the EHS method was applied. Furthermore, element A refers to the element at the pole of the concave part of the roller path profile as shown in Figs. 11, 12, and 14.

According to Fig. 20, $\varepsilon_{\mathrm{h}}=\varepsilon_{\mathrm{h1}}+\varepsilon_{\mathrm{h2}}=-0.19$ and $\varepsilon_{\mathrm{h0}}=\varepsilon_{\mathrm{h}}/2=-0.095$. Since the hoop strains of EHS were closest to $\varepsilon_{\mathrm{h0}}$ among the three methods, $\varepsilon_{\mathrm{h1,EHS}}$ and $\varepsilon_{\mathrm{h2,EHS}}$ can be treated as $\varepsilon_{\mathrm{h0}}$ in Eq. (12). According to Eqs. (19) and (20), $\varepsilon_{\mathrm{h1,EDD}}\approx\varepsilon_{\mathrm{h0}}+\Delta\varepsilon_{\mathrm{h,EDD}}$ and $\varepsilon_{\mathrm{h2,EDD}}\approx\varepsilon_{\mathrm{h0}}-\Delta\varepsilon_{\mathrm{h,EDD}}$ ($\Delta\varepsilon_{\mathrm{h,EDD}}>0$). The hoop strains of EPA can be treated in the same way.

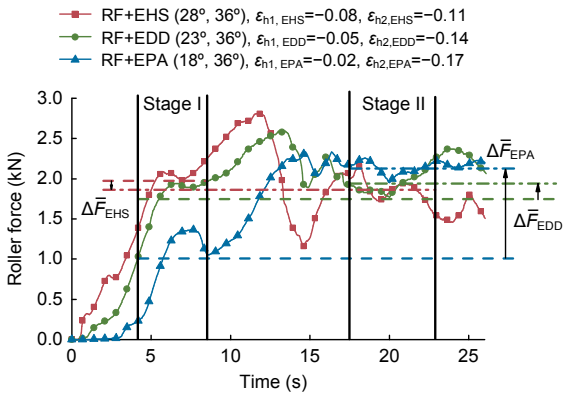

Fig. 20 Simulation results of roller force history and variations of average roller forces between two passes using different deformation allocation methods

As shown in Fig. 20, the order of deviations of average forces is identical to the order of gaps of hoop strains between the passes:

$$\overline{F}_{\mathrm{II,EPA}}-\overline{F}_{\mathrm{I,EPA}}>\overline{F}_{\mathrm{II,EDD}}-\overline{F}_{\mathrm{I,EDD}}>\overline{F}_{\mathrm{II,EHS}}-\overline{F}_{\mathrm{I,EHS}}.$$

According to the above theoretical analysis, the inconsistency of hoop strains between the passes was the cause of the widened disparities of roller forces of EDD and EPA.

Furthermore, an extra increment of total radial strain can be observed in Fig. 21a, i.e., $\varepsilon_{\mathrm{r1,EPA}}+\varepsilon_{\mathrm{r2,EPA}}>\varepsilon_{\mathrm{r1,EDD}}+\varepsilon_{\mathrm{r2,EDD}}>\varepsilon_{\mathrm{r1,EHS}}+\varepsilon_{\mathrm{r2,EHS}}$. As demonstrated by inequality (26), the additional radial strains of EPA and EDD were created by the widened deviation of roller forces between the passes.

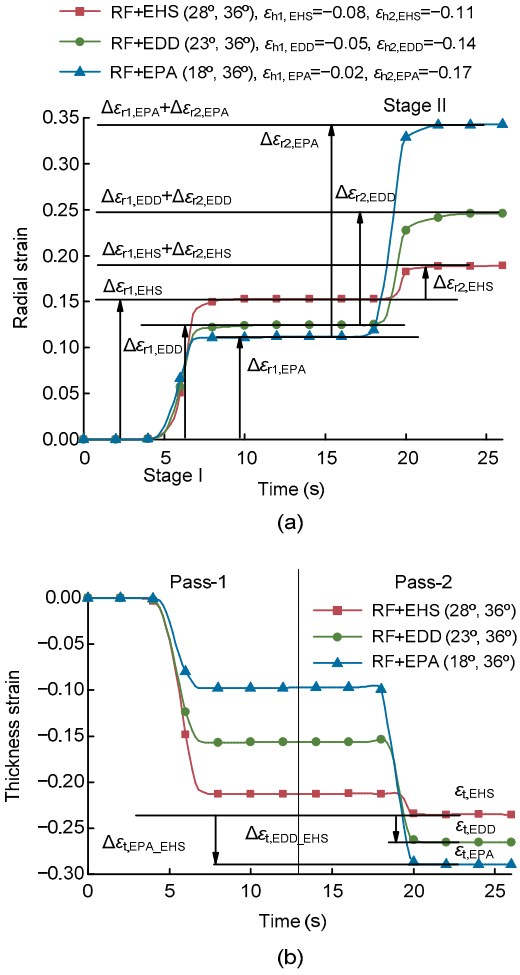

Fig. 21 Simulation results of radial (a) and thickness (b) strain histories of element A using different deformation allocation methods in two passes

In addition, the total radial strain of EPA was larger than that of EDD as the deviation of roller forces was larger when the EPA method was applied.

According to the above theoretical analysis, extra increments of total radial strains of EDD and EPA would lead to additional increment of thickness strains, i.e., $\Delta\varepsilon_{t,EDD\_EHS}$ and $\Delta\varepsilon_{t,EPA\_EHS}$ in Fig. 21b.

Thus, the corresponding theoretical analysis and speculations expressed in inequalities (26)–(28) have been verified.

As displayed in Fig. 18, the order of wall thicknesses is EHS>EDD>EPA, which, according to the above theoretical and numerical studies, could be explained by the differences of consistencies of the hoop strains between passes.

To verify the above theoretical analysis, forming experiments were conducted, of which the slant angles and results of part wall thickness were demonstrated in Fig. 22. Straight lines were applied as the roller paths so that average hoop strains could be qualified by slant angles.

It is shown in Fig. 22 that when average hoop strains were identical among passes, wall thickness was better maintained, thus verifying the validity of the above theoretical analysis.

In conclusion, for a die-less spinning process, the deformation should be evenly allocated among the passes to prevent the part wall thickness from excessive thinning and this is called the 'uniform allocation principle for maintaining wall thickness'.

6 Final pass prior & equal hoop strain, FP & EHS allocation method

Although the shape deviation of the EPA method was the smallest, the part wall was also seriously thinned, as illustrated in Fig. 18. By contrast, the wall thickness of the EHS method was acceptable although its shape deviation was large.

Moreover, as the contour of a spun part was directly formed in the final pass, taking into account the 'large deformation principle for restraining shape deviation', final-pass deformation was chosen as the parameter for further optimizing the EHS method.

First, the proportion factor p_F was proposed to denote the ratio of the average hoop strain of the final pass $\bar{\varepsilon}_{hF}$ to that of the whole spinning process $\bar{\varepsilon}_h$:

$$p_F = \bar{\varepsilon}_{hF} / \bar{\varepsilon}_h . \quad (29)$$

Forming experiments were carried out with p_F increased from 30% to 70%; the final-pass profile is shown in Fig. 4 with α_t as 50°.

According to Fig. 23, the shape deviation was monotonically decreased when the final-pass deformation was increased from 25% to 50%.

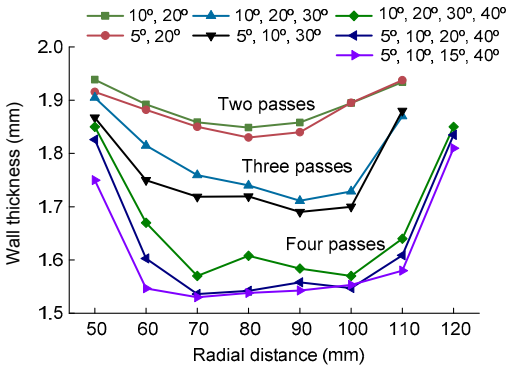

Fig. 22 Comparison of part wall thicknesses with even and uneven deformation allocations under linear roller paths

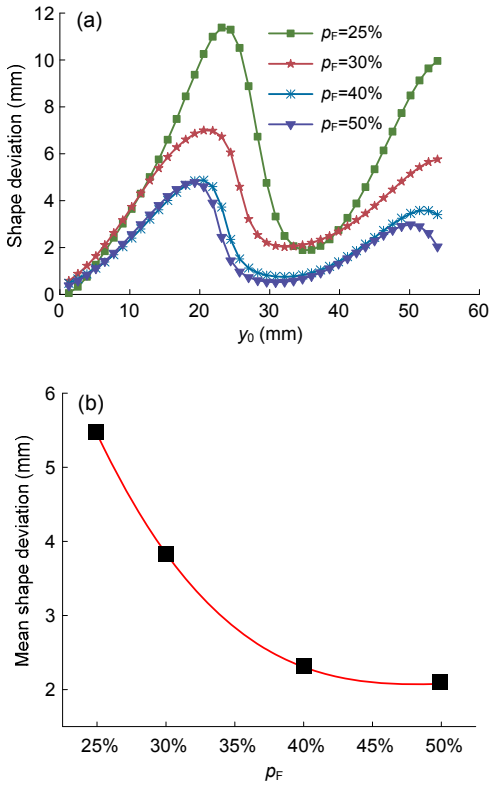

Fig. 23 Shape deviations under different p_F

(a) Shape deviations along radial direction; (b) Mean shape deviations

Furthermore, the shape deviation was effectively reduced when p_F was increased from 25% to 40%; by contrast, when p_F was increased from 40% to 50%, the shape deviation was not reduced so obviously. As demonstrated in Fig. 24, the thickness of the part wall was also monotonically decreased with the increment of p_F; eventually, circumferential cracking on the part wall occurred when p_F was larger than 60%, as shown in Fig. 25.

As a conclusion, the shape deviation of a spun product could be reduced by increasing the deformation of the final pass; however, the thickness of the part wall would also be decreased.

Consequently, there should be an optimum range of p_F to improve the comprehensive quality: First, the upper limit of p_F should be designed to make sure that the quantity of wall thickness is acceptable; under this premise, p_F should be set as large as possible to restrain shape deviations.

For the spinning process in this study, the optimum range is approximately 30%–40%; a more accurate number largely depends on the wall thickness specification for the product. This allocation method is denoted by FP & EHS, in which the final pass was given priority consideration and the EHS method was then applied in earlier passes under the condition that the RF processing method was applied.

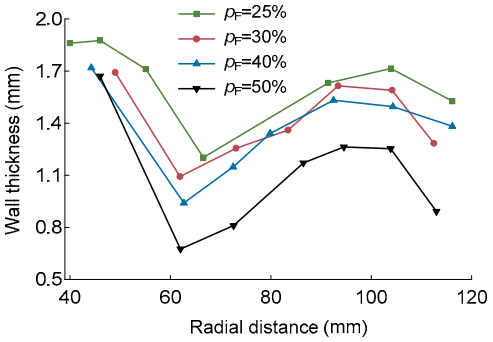

Fig. 24 Wall thicknesses of the parts under different p_F

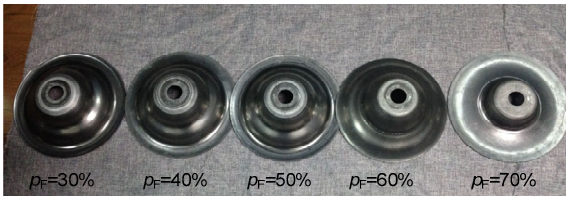

Fig. 25 Part qualities under different p_F

7 Discussion

As demonstrated in Fig. 26, the effects of roller path profiles and deformation allocations on shape deviations and wall thicknesses were confirmed. Slant angles and roller path profiles of the experiments in Fig. 26 are listed in Table 4.

Additionally, for the experiments conducted to investigate the roller path profiles, deformation

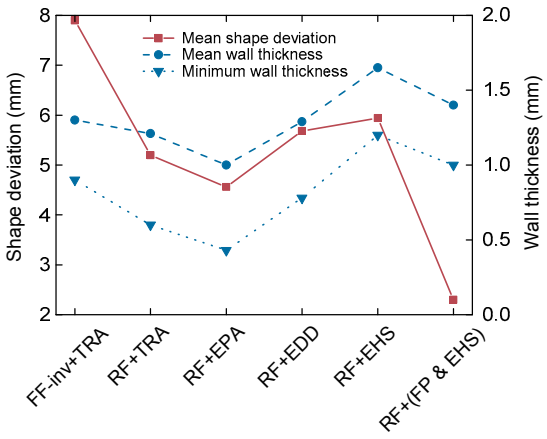

Fig. 26 Comparison of pass scheduling methods

Table 4 Experimental settings for the comparison of different pass scheduling methods

Method	Slant angles (°)	Roller path profile of former passes	Deformation allocation method	Forming quality	
				Shape precision	Wall thickness keeping capability
FF-inv+TRA	20, 30, 40, 50	Involute	Traditional way	−−	+
RF+TRA	20, 30, 40, 50	Desired shape	Traditional way	+	+
RF+EPA	12.5, 25, 37.5, 50	Desired shape	EPA	+	−
RF+EDD	23, 35, 43, 50	Desired shape	EDD	−	++
RF+EHS	28, 36, 44, 50	Desired shape	EHS	−	+++
RF+(FP & EHS)	22, 28, 36, 50	Desired shape	FP & EHS	++	++

'+' is used if the scheduling method has a positive effect on the product quality and '−' if the effect is negative

allocations were developed referring to the traditional allocation way (TRA) proposed by Hayama *et al.* (1970).

When the RF method was applied, the profile of the former-pass roller path was identical to the desired shape; hence, the shape deviation was obviously reduced. Thereby, the RF method was chosen as the processing method, given that low-dimensional precision is the major problem in die-less spinning.

Using the EHS method can help preserve the part wall thickness from excessive thinning; however, the shape deviation will be increased. By applying the RF+(FP & EHS) pass schedule, the shape deviation of the formed part was effectively restrained while the part wall was also better maintained when compared with the traditional FF-inv+TRA schedule.

8 Conclusions

Based on the theoretical analysis and experimental research, multi-pass scheduling methods, of which roller path profiles and deformation allocations are the two key parameters, have been investigated in this study. The following conclusions can be drawn:

Both roller path profiles and deformation allocations influence shape deviations and part wall thicknesses.

As suggestions for optimal design of roller path profiles, the 'similar geometry principle for restraining shape deviation' and the 'small curvature principle for maintaining wall thickness' were presented. Comparing the effects of the four processing methods on reducing the shape deviation, the order is RF> GF>FF-lin>FF-inv; comparing their effects on maintaining the part wall, the order is FF-inv> FF-lin>GF>RF.

For deformation allocations, the 'large deformation principle for restraining shape deviation' and the 'uniform allocation principle for maintaining wall thickness' were proposed. Comparing the effects of three deformation allocation methods on reducing the shape deviation under the condition of using the RF method, the order was RF+EPA>RF+EDD>RF+ EHS; comparing their effects on maintaining the part wall thickness, the order was RF+EHS>RF+EDD> RF+EPA.

The RF+(FP & EHS) scheduling method was proposed to improve the comprehensive quality of products: giving priority consideration to dimensional precision, the RF processing method was chosen to restrain the shape deviation; given priority in deformation allocation, the final-pass deformation was 30%–40% of the total. Furthermore, the EHS allocation method was applied in the former passes for maintaining part wall thickness.

For the purpose of focusing on roller path profiles and deformation allocations, backward passes were not taken into investigation in this paper; they should be included in further research.

References

El-Khabeery, M.M., Fattouh, M., El-Sheikh, M.N., *et al*., 1991. On the conventional simple spinning of cylindrical aluminum cups. *International Journal of Machine Tools and Manufacture*, **31**(2):203-219. http://dx.doi.org/10.1016/0890-6955(91)90005-N

Hayama, M., Kudo, H., Shinokura, T., 1970. Study of the pass schedule in conventional simple spinning. *Bulletin of JSME*, **13**(65):1358-1365. http://dx.doi.org/10.1299/jsme1958.13.1358

Jia, Z., Han, Z.R., Xu, Q., *et al*., 2015. Effects of processing parameters on the surface quality of square section die-less spinning. *The International Journal of Advanced Manufacturing Technology*, **80**(9):1689-1700. http://dx.doi.org/10.1007/s00170-015-7055-9

Kang, D.C., Gao, X.C., Meng, X.F., *et al*., 1999. Study on the deformation mode of conventional spinning of plates. *Journal of Materials Processing Technology*, **91**(1-3): 226-230. http://dx.doi.org/10.1016/S0924-0136(98)00447-6

Kawai, K., Yang, L.N., Kudo, H., 2001. A flexible shear spinning of truncated conical shells with a general-purpose mandrel. *Journal of Materials Processing Technology*, **113**(1-3):28-33. http://dx.doi.org/10.1016/s0924-0136(01)00630-6

Kawai, K., Yang, L.N., Kudo, H., 2007. A flexible shear spinning of axi-symmetrical shells with a general-purpose mandrel. *Journal of Materials Processing Technology*, **192-193**:13-17. http://dx.doi.org/10.1016/j.jmatprotec.2007.04.008

Kopp, R., Wiegels, H., 1998. Einführung in Die Umformtechnik. Kang, Y., Hong, Z., translators, 2010. Higher Education Press, Beijing, China (in Chinese).

Li, Y., Wang, J., Lu, G.D., *et al*., 2014. A numerical study of the effects of roller paths on dimensional precision in die-less spinning of sheet metal. *Journal of Zhejiang University-SCIENCE A (Applied Physics & Engineering)*, **15**(6):432-446. http://dx.doi.org/10.1631/jzus.A1300405

Lin, X.J., Ge, T., Wang, J., *et al*., 2015. Numerical investiga-

tion of effects of deformation allocation on multi-pass conventional spinning process of curvilinear generatrix parts. *Proceedings of the Institution of Mechanical Engineers, Part C: Journal of Mechanical Engineering Science*, **229**(18):3299-3307. http://dx.doi.org/10.1177/0954406215570384

Liu, C.H., 2007. The simulation of the multi-pass and die-less spinning process. *Journal of Materials Processing Technology*, **192-193**:518-524. http://dx.doi.org/10.1016/j.jmatprotec.2007.04.021

Liu, J.H., Yang, H., Li, Y.Q., 2002. A study of the stress and strain distributions of first-pass conventional spinning under different roller-traces. *Journal of Materials Processing Technology*, **129**(1-3):326-329. http://dx.doi.org/10.1016/S0924-0136(02)00682-9

Music, O., Allwood, J.M., Kawai, K., 2010. A review of the mechanics of metal spinning. *Journal of Materials Processing Technology*, **210**(1):3-23. http://dx.doi.org/10.1016/j.jmatprotec.2009.08.021

Polyblank, J.A., Allwood, J.M., 2015. Parametric toolpath design in metal spinning. *CIRP Annals—Manufacturing Technology*, **64**(1):301-304. http://dx.doi.org/10.1016/j.cirp.2015.04.077

Quigley, E., Monaghan, J., 2000. Metal forming: an analysis of spinning processes. *Journal of Materials Processing Technology*, **103**(1):114-119. http://dx.doi.org/10.1016/S0924-0136(00)00394-0

Sugita, Y., Arai, H., 2015. Formability in synchronous multipass spinning using simple pass set. *Journal of Materials Processing Technology*, **217**:336-344. http://dx.doi.org/10.1016/j.jmatprotec.2014.11.017

Wang, L., Long, H., 2011. A study of effects of roller path profiles on tool forces and part wall thickness variation in conventional metal spinning. *Journal of Materials Processing Technology*, **211**(12):2140-2151. http://dx.doi.org/10.1016/j.jmatprotec.2011.07.013

Wang, L., Long, H., 2013. Roller path design by tool compensation in multi-pass conventional spinning. *Materials & Design*, **46**:645-653. http://dx.doi.org/10.1016/j.matdes.2012.10.048

Wong, C.C., Dean, T.A., Lin, J., 2003. A review of spinning, shear forming and flow forming processes. *International Journal of Machine Tools and Manufacture*, **43**(14):1419-1435. http://dx.doi.org/10.1016/S0890-6955(03)00172-X

Xia, Q., Xiao, G., Long, H., *et al*., 2014. A review of process advancement of novel metal spinning. *International Journal of Machine Tools and Manufacture*, **85**:100-121. http://dx.doi.org/10.1016/j.ijmachtools.2014.05.005

中文概要

题　目： 无芯模旋压道次规划方法研究

目　的： 通过优化无芯模旋压轨迹提高成形件形状精度，同时保持壁厚以防止过度减薄。

创新点： 针对轨迹形状设计，提出利于形状误差抑制的“几何相似性原则”和利于壁厚保持的“小曲率原则”。针对道次间距设计，提出利于形状误差抑制的终道次“大变形量原则”和利于壁厚保持的“变形量均匀分配原则”。

方　法： 首先，根据不同的前道次轨迹形状与目标件复杂轮廓形状的结合衍生出四种成形方式（表 1）。通过试验比较不同成形方式对成形件形状精度和壁厚的影响。而后比较等道次倾角差（EPA）、等外径差（EDD）和等平均环向应变（EHS）成形量分配方法对成形质量的影响（图 13~16）。最后，根据终道次对成形质量的关键性影响，提出基于终道次优先的等平均径向应变道次轨迹规划方法。

结　论： 基于终道次优先的等平均径向应变道次轨迹（RF+(FP & EHS)）规划方法，能够在有效抑制形状偏差和提高形状精度的同时较好地保持壁厚以防止过度减薄，是一种较优的道次轨迹规划方法。

关键词： 无芯模旋压；道次规划；形状偏差；旋轮轨迹；变形量分配